Parametrization of the cumulant lattice Boltzmann method for fourth order accurate diffusion Part II: Application to flow arou....

Article *in* Journal of Computational Physics · July 2017

DOI: 10.1016/j.jcp.2017.07.004

CITATIONS
2

READS
167

3 authors:

Martin Geier
Technische Universität Braunschweig
37 PUBLICATIONS **422** CITATIONS
SEE PROFILE

Andrea Pasquali
FluiDyna GmbH
9 PUBLICATIONS **67** CITATIONS
SEE PROFILE

Martin Schönherr
Technische Universität Braunschweig
10 PUBLICATIONS **128** CITATIONS
SEE PROFILE

Parametrization of the cumulant lattice Boltzmann method for fourth order accurate diffusion Part II: application to flow around a sphere at drag crisis[1]

Martin Geier[a,*], Andrea Pasquali[a], Martin Schönherr[a]

[a]*TU Braunschweig, Institute for Computational Modeling in Civil Engineering (iRMB),Braunschweig, Germany*

Abstract

The optimized cumulant lattice Boltzmann method with fourth order accurate diffusion is used to simulate the flow around a sphere up to Reynolds number 10^6. The drag crisis is well captured by the method. We demonstrate with our results that the drag crisis corresponds to an almost discrete jump in the flow conditions. The intermediate values of drag in a small range of Reynolds numbers around the drag crisis observed in averaged data sets are found to originate from the flow switching between the high and the low drag conditions. Around the critical Reynolds number, the time spent in the low drag condition increases with the Reynolds number such that the average drag curve has a finite steepness.

Keywords: lattice Boltzmann, cumulants, drag crisis, multiple relaxation times, fourth order

1. Introduction

This paper is the second part in a series of two on a high fidelity cumulant lattice Boltzmann model with fourth order accurate diffusion for sufficiently small viscosity. Part one of the series [1] shows, based on the cumulant lattice Boltzmann model [2, 3, 4, 5, 6], how the relaxation parameters have to be selected in order to obtain fourth order accuracy in diffusion. It is found that fourth order accuracy in diffusion cannot be enforced by the relaxation rates alone and two small modifications of the collision operators for fourth order cumulants have to be added.

The main motivation for increasing the order of convergence of the cumulant lattice Boltzmann model is in the high computational cost associated with the simulation of turbulent flow. High order methods make better use of computational resources than low order methods. The benefit of this is particularly evident when deployed on large scale architectures. Previous attempts of increasing the convergence order of the lattice Boltzmann method by specific parametrization [7] were limited to Stokes flow and very high viscosity such that they bear no relevance to the simulation of turbulent flow. The method of [1] is the first to eliminate one class of leading errors completely in the viscosity regime most relevant for the simulation of turbulent flow. The aim of the current paper is to demonstrate that the high fidelity of the method predicted in [1] and demonstrated for some academic test cases persists under conditions relevant for industrial computational fluid dynamics. The example we chose is the flow around a sphere at Reynolds numbers large enough to trigger the drag crisis. For further discussions on the optimally parametrized cumulant method and a recipe for its implementation the reader is directed to the first part of the series [1]. The method used here disregards the correction in advection [8] such that advection is not fourth order accurate.

2. Flow around a sphere at drag crisis

We demonstrate the abilities of the cumulant lattice Boltzmann method with fourth order accurate diffusion by simulating flow around a sphere in the Reynolds number range 10^4 to 10^6. This flow is particularly suitable for the

[1] Article in press, Journal of Computational Physics 2017 doi:10.1016/j.jcp.2017.07.004

[*] Corresponding author at: iRMB Pockelsstr. 3, 38106 Braunschweig, Germany. Tel: +49 531 391 94518; Fax: +49 531 391 94511.
Email address: geier@irmb.tu-bs.de (Martin Geier)

demonstration of our model's high fidelity under fully turbulent conditions since the character of this flow changes drastically somewhere near $Re \sim 250000$. Below this critical value, the drag coefficient is almost constant over several orders of magnitude in Reynolds number. At the critical Reynolds number the drag coefficient drops to about one-fifth of its previous value. This phenomenon is known as the drag crisis and it is a problem of high scientific as well as practical interest. A drag crisis also occurs for flow around a circular cylinder at a similar Reynolds number. The drag crisis was first described more than 100 years ago by Eiffel [9] and Wieselberger [10] and has since been an active field of experimental research [11, 12, 13]. Due to the high Reynolds numbers involved the full three dimensional problem has only recently become accessible to numerical investigation [14, 15, 16, 17, 16, 18]. It should be noted however that the first numerical results capturing the drag crisis in two dimensions were obtained 30 years ago [19]. The first demonstration of the drag crisis with the lattice Boltzmann method in 2D was presented by Schönherr et al. [20] using a cascaded lattice Boltzmann model [21, 22**?** , 23].

While the drag crisis can be described phenomenologically, the driving mechanism behind it is not well understood and a satisfactory explanation is still missing. At the drag crisis dissipation suddenly drops by 80% [12], which has obvious implications in many engineering disciplines, especially in the context of energy efficiency. The phenomenon is also of importance for numerics since, if the drag crisis is not accurately captured by a simulation method, the simulation will be qualitatively wrong. For example, if a numerical method fails to reproduce the drag crisis for a cylindrical object it will over-predict the dissipation by some 400%. It is therefore essential for us to demonstrate here that our method correctly predicts the drag crisis.

Due to the fact that the mechanisms of the drag crisis are only partly understood and due to the high Reynolds numbers involved, the drag crisis is still difficult to use as a general benchmark. In particular, the exact value of the critical Reynolds number is not known. Measurements of the drag crisis show a wide scatter for the critical Reynolds number and for the actual reduction in drag [13].

3. Simulation setup

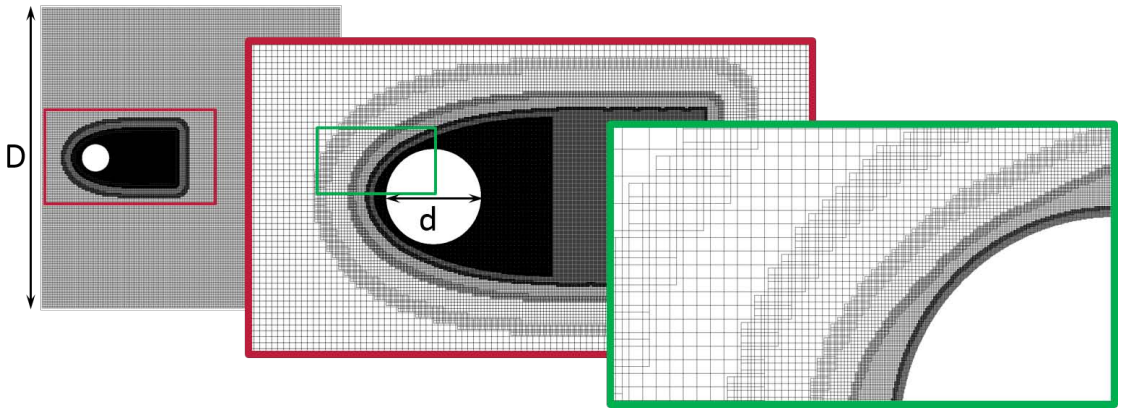

Figure 1: Cut through the grid used for the simulation of the drag crisis (medium resolution). The simulation domain is a cubic box of length $D \times D \times D$. The sphere is embedded in six layers of exponentially refined grids. The picture on the left shows the entire simulation domain and the two on the right show successive details. The grid refinement technique uses an overlap region for interpolation between the grids, which is visible on the right. The finest grid is used directly on the surface of the sphere. The wake region is not well resolved since we are primarily interested in the dynamics of the flow near the surface of the sphere.

We consider a sphere of diameter d in a cubic box with side length $D = 11d$ (see Fig. 1). The center of the sphere is located $2d$ from the side of the box in negative x-direction. All faces of the cube expect of the one in positive x-direction have velocity boundary conditions imposing a constant velocity. The outflow in positive x-direction is implemented as a non-reflective outflow boundary condition [2]. We use successively refined Cartesian grids with compact quadratic interpolation at the grid interfaces for the simulation [24, 25, 26] combined with the Esoteric Twist data structure [27]. The gird (shown in Fig. 1) was generated with LBMHexMesh [28, 29]. In total, six grid levels are used with $\Delta x_i = 2^{-i}\Delta x_0$ for $i \in \{0, 1, 2, 3, 4, 5\}$. The finest grid level is clustered around the surface of the sphere.

We conjecture that the wake some distance behind the sphere is not relevant for the drag crisis and so this area is not well resolved. The thickness of the laminar boundary layer is estimated *a priori* to be $\delta/d \approx 3Re^{-1/2}$ [30, 31] with the Reynolds number defined with respect to the diameter of the sphere. Estimating that the drag crisis occurs around $Re \sim 250000$ the sphere diameter is required to span at least 500 nodes of the finest mesh to ensure that at least three of these grid nodes are within the boundary layer. It should be noted that super-critical flow can be simulated on much coarser grids, not resolving the boundary layer, when using a partial slip boundary condition [32, 33]. Here, however, we use the drag crisis as a benchmark and simulate the flow without any assumptions and no turbulence model or wall model.

We study the drag crisis with three different resolutions. The coarse grid has $410\Delta x_5$ across the diameter of the sphere, the medium grid has $512\Delta x_5$ and the fine grid has $640\Delta x_5$ across the diameter. The coarse grid is hence seen to be under-resolved for the critical Reynolds number and even the medium and fine resolution cannot fully resolve the boundary layer, especially for Reynolds numbers beyond the critical value. The three grids have 40,769,886, 73,855,027 and 133,438,032 nodes, respectively. No higher resolution was considered due to the high computational cost of further refinement. The surface of the sphere was discretized with compact interpolated bounce back boundary conditions as in [2]. The inflow velocity for the fine grid was $u_0 = 0.01\Delta x_0/\Delta t_0$ and the inflow velocity for the other resolutions was obtained from diffusive scaling as $u_0 = 0.0125\Delta x_0/\Delta t_0$ for the medium and $u_0 = 0.015625\Delta x_0/\Delta t_0$ for the coarse grid, respectively. It should be noted that these inflow velocities are about seven times smaller than the one used in [2]. As we discussed in the first part of the series [1], in the absence of the optimized parameters the accuracy of the cumulant method can actually deteriorate for smaller Mach numbers (a property shared also by other lattice Boltzmann methods). In the case of the optimized cumulant method, the error is observed to decrease with decreasing Mach number. Even though decreasing the Mach number is equivalent to decreasing the time step, decreasing the Mach number might actually increase computational efficiency. This is so since the computational cost increases only linearly with a decreasing time step while it increases with the fourth power of a decreasing grid spacing. For a larger Mach number, a finer grid is required to keep the same accuracy. It is hence seen that it is much more favorable to decrease the error by decreasing the time step than by decreasing the grid spacing.

The simulation was run for $90000\Delta t_0$ for the fine case and for $60000\Delta t_0$ for the other two cases. All simulations were run on multiple GPGPUs in single precision.

4. Results

To visualize the drag crisis we measure the drag force F_D acting on the sphere in flow direction by the momentum exchange method for stationary objects [38]. The drag coefficient c_D is computed from:

$$c_D = \frac{8F_D}{\rho u_0^2 \pi d^2}, \tag{1}$$

where ρ is the mean density of the fluid. In the Reynolds number range of interest, the flow is completely turbulent and the drag undergoes a strong initial transient and remains to be a function varying strongly in time. In order to discard the initial transient we average the c_D value in the interval from $1.8 \times 10^6 \Delta t_5$ to $2.88 \times 10^6 \Delta t_5$ on the fine grid and use diffuse scaling to select the same time window for the medium and coarse simulation. The main flow covers a distance of 16.875 sphere diameters in this time window. It should be noted that this is a compromise regarding the large computational cost of the simulation. The averaging time is too short to eliminate the intermittent turbulent fluctuations but longer averaging times were not feasible given that the medium resolution simulations took four days for each Reynolds number. The averaged drag coefficient versus Reynolds number is depicted in Fig. 2 together with various experimental measurements. The drag crisis is seen in all three resolutions for the optimized cumulant method. Below the critical Reynolds number the c_D value is more or less independent of the Reynolds number. Above a critical Reynolds number the drag coefficient drops suddenly to a much lower value. We note that, compared to experimental values, the critical Reynolds number is over-predicted on the coarse grid while the reduction in drag is under-predicted. For the medium and fine resolution both the critical Reynolds number and the reduction of the drag are close to experimental values with the fine resolution predicting a lower value for the critical Reynolds number which is also lower than the experimental critical Reynolds number. A lower value for the critical Reynolds number compared to experiments was also observed in the simulations of Muto et al. [15] and in those by Chopra and Mittal

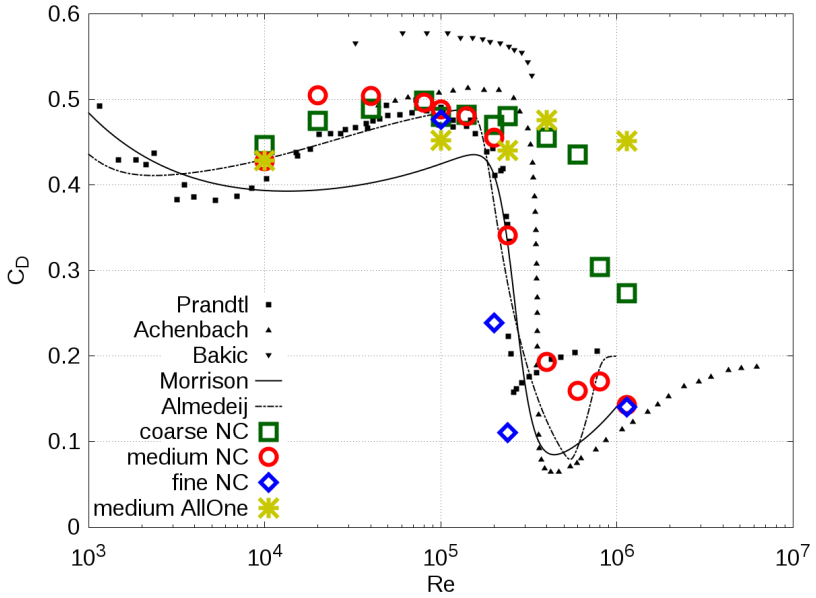

Figure 2: Time averaged drag coefficient versus Reynolds number. We compare our simulations for the new cumulant method (NC) with experimental data and regression functions for the standard drag curve. It is important to note that the experimental data shows a wide scatter, such that an exact correspondence between the simulation and any of the experiments is not expected. We observe that the medium and fine simulations are close to the curves obtained from experiments. The drag crisis is also seen in the coarse simulation albeit with a larger deviation from the experimental data. Note that, for the higher Reynolds numbers, the boundary layer is not well resolved with the coarse resolution and that we did not use a turbulence or wall model. We also display the results of the original cumulant method with the relaxation rates for third order cumulants set to one on a medium resolution (asterisk). It is observed that the non-optimized cumulant method does not predict the drag crisis at this resolution. The experimental data is taken from Achenbach [12], Prandtl [34] and Bakic [35]. The regression functions are taken from Morrison [36] and Almedij [37].

[17] for the cylinder. A reason for the discrepancy could be that the discretized surface of the sphere is not perfectly smooth as our boundary condition models only the distance between the last fluid nodes and the surface but does not account for the curvature.

In contrast to the results obtained with the optimized cumulant method the cumulant method with the relaxation rates of the third order cumulants set to one does not predict the drag crisis even at a Reynolds number of one million. This is despite the fact that the sub-critical drag coefficient is accurately captured by the non-optimized cumulant method. In the first part of this series [1], we compared the accuracy and convergence order of the two different versions of the cumulant method and we could demonstrate significant improvements with regard to accuracy using the proposed parametrization. It is expected that any correct method would predict the drag crisis with enough resolution. However, in the case of the drag crisis, the requirements on the resolution are difficult to fulfill unless a high order method is employed.

While our results from the medium and fine resolution are clearly closer to the experimental data than the coarse simulation, no clear convergence can be determined from the three resolutions. This must be attributed not only to the fact that the simulations do not resolved the Kolmogorov scale but also to the statistical nature of the result. It is instructive to compare the simulation results to the scatter between the different experiments.

In Fig. 3 we also show the y^+ value for the first node next to the surface of the wall. We calculate it as:

$$y^+ \approx \Delta x_5 \sqrt{\frac{|\vec{u}(l)|}{\nu l}}. \tag{2}$$

Here ν is the kinematic viscosity. We evaluate the velocity $\vec{u}$ at a distance $l = 2\Delta x_5$ from the surface of the sphere and approximate the gradient of the velocity by dividing by this distance. The finite distance is necessary for the post-processing software to recover a closed surface of a sphere by interpolation between valid grid nodes. We note that the procedure adds some uncertainty to the result. We also assume that the contribution of the velocity normal to

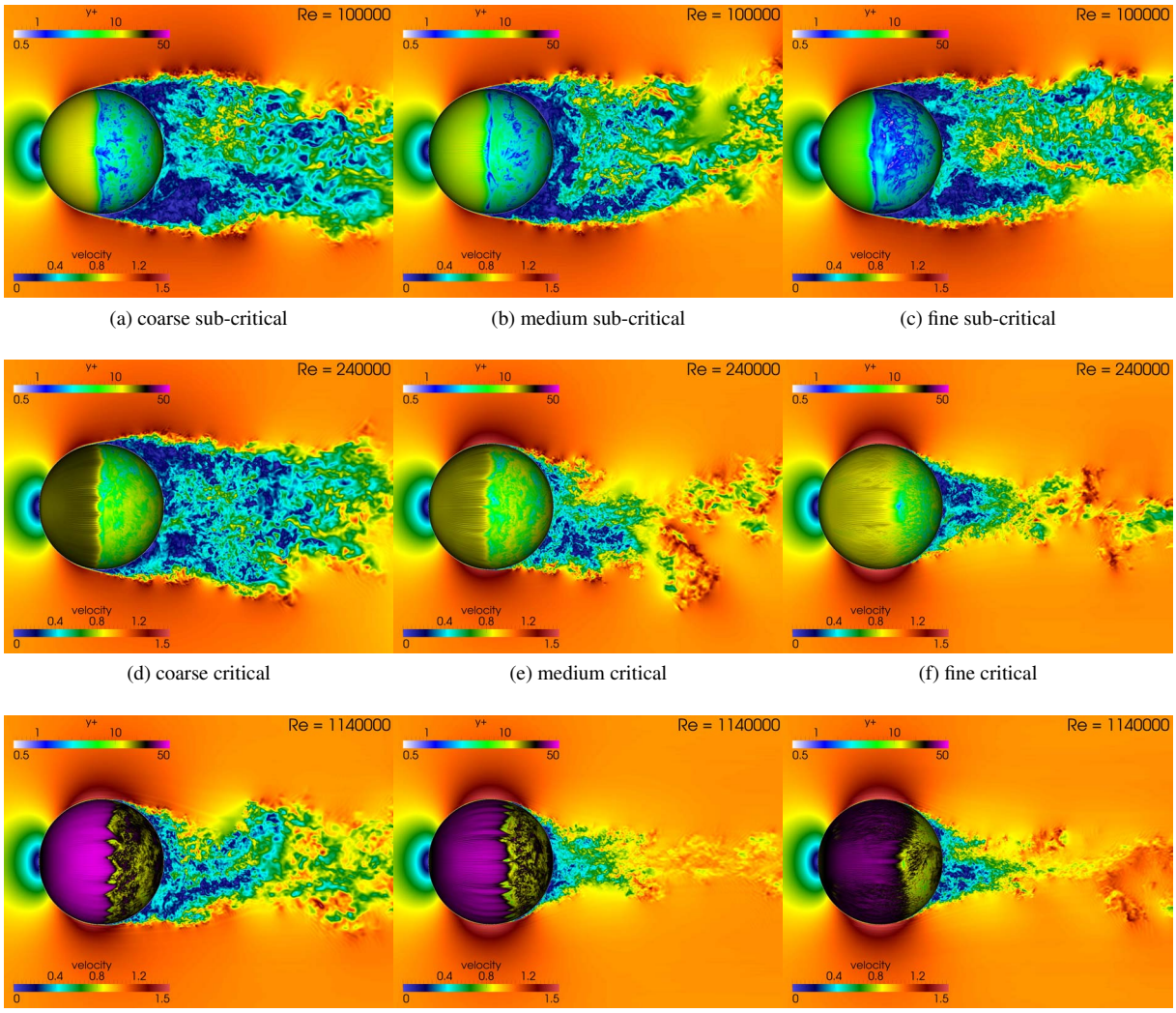

(a) coarse sub-critical (b) medium sub-critical (c) fine sub-critical

(d) coarse critical (e) medium critical (f) fine critical

(g) coarse super-critical (h) medium super-critical (i) fine super-critical

Figure 3: Velocity field above (top), at (middle) and below (bottom) drag crisis at Reynolds number 100000, 240000 and 1140000, respectively. The velocity is scaled with the inlet velocity ($u_0 = 1$). The color on the surface of the sphere depicts the dimensionless wall distance y^+ value in logarithmic scale. The left, middle and right pictures are the results from the coarse, medium and fine grids, respectively.

the surface of the sphere is negligible and that $|\vec{u}|$ is the magnitude of the tangential velocity. It is seen from Fig. 3 that none of the used grids is able to resolve the boundary layer at the critical Reynolds number. Even sufficiently below the critical Reynolds number at $Re = 100000$ the value of y^+ at the turbulent back side of the sphere is about 3 for the fine grid and above 6 for the coarse grid. Around the critical Reynolds number, at $Re = 240000$ where turbulence already starts on the front side of the sphere we get $y^+ > 10$ even for the fine grid and it reaches 20 for the coarse grid. At this Reynolds number the drag crisis is still captured accurately at least on the medium and fine grids. The method is seen to be robust under severe under-resolution. The highest y^+ values observed on the coarse grid at $Re = 1140000$ are $y^+ \approx 48$. The drag crisis is still qualitatively captured at this poor resolution.

It is instructive to ask whether the observation of the drag crisis in our simulation could be a result of accidental slip which arises from a hereto unknown interaction between the optimized collision rates and the one-point, second order accurate boundary conditions which we adopted from Appendix E in [2]. It is known that the drag crisis can be obtained by simulating the flow around a sphere or a cylinder even on very coarse grids when a partial slip boundary

condition is applied [32, 33] and our results could originate from a similar effect. However, contrary to our results a partial slip velocity would trigger the drag crisis independent from the Reynolds number. For example, Hoffman [32, 33] either obtained the pre-critical or post-critical state depending on which amount of slip he applied. He did not recover the actual transition as a function of the Reynolds number as we do.

Our simulation allows us to give a phenomenological description of the drag crisis (see Fig. 3). Below the critical Reynolds number, the wake behind the sphere is divergent (it becomes broader the further it travels from the sphere). Above the critical Reynolds number the wake converges and becomes very narrow behind the sphere. At the same time a pressure maximum emerges on the wake side of the sphere that forces the sphere in the flow direction.

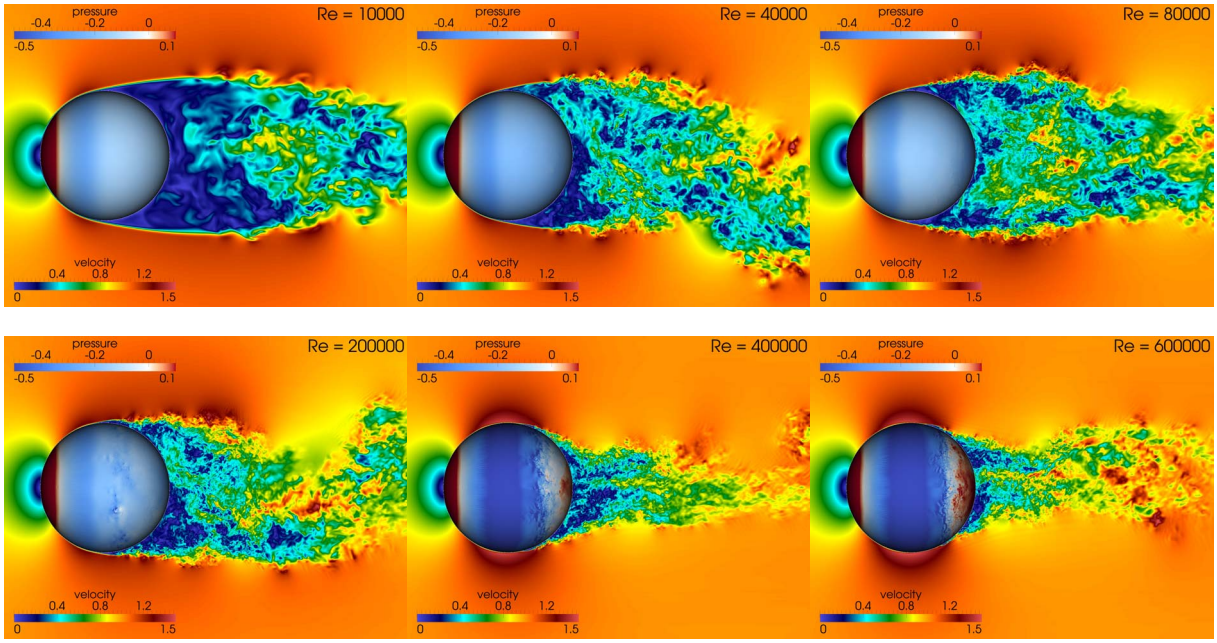

Figure 4: Comparison between the velocity field and surface pressure for different Reynolds number using the medium grid resolution. The velocity is scaled with the inlet velocity ($u_0 = 1$). Below the drag crisis, for several orders of magnitude in the Reynolds number, the flow separates from the sphere at an angle smaller than 90, that is in the hemisphere facing the flow. Above drag crisis the separation point has jumped to the hemisphere pointing away from the flow. Below the drag crisis, the wake is diverging and above the drag crisis it is converging. Above drag crisis a pressure maximum emerges on the wake side of the sphere that forces the sphere in the flow direction and thereby reducing the drag significantly.

Fig. 4 shows the development of the wake over more than one order of magnitude in Reynolds number. While the vortices in the wake are getting smaller for larger Reynolds number, the separation angle of the wake is hardly affected by the Reynolds number until the critical Reynolds number is reached. In Fig. 5 we display the three dimensional structure of the wake by plotting the contour of the Q-criterion [39].

It is an interesting question whether the transition between the high drag state and the low drag state is sudden or continuous. Most experimental data shows a steep transition but with sufficiently many data points on the slope to support the theory of a smooth transition. However, one must keep in mind that the drag curve is obtained as a temporal average and that c_D fluctuates considerably in time. For the case of a circular cylinder Chopra and Mittal [17] attributed the drag crisis to the existence of a laminar separation bubble. They showed with their simulation that the laminar separation bubble does not exist below the critical Reynolds number and that it exists most of the time above the critical Reynolds number. In the transitional regime, the laminar separation bubble was intermittent: it existed for a fraction of the time. It can hence be said that, in the transition regime, the flow is sometimes super-critical and sometimes sub-critical, which on average results in a drag coefficient between the lower and the upper value. Similar conclusions have been drawn from experimental results. Miau et al. [40] observed pressure fluctuations at a circular cylinder in the critical regime with a time scale one order of magnitude larger than the time scale of the vortex shedding. Looking at the time series of our own results as depicted in Fig. 6 we could draw a similar

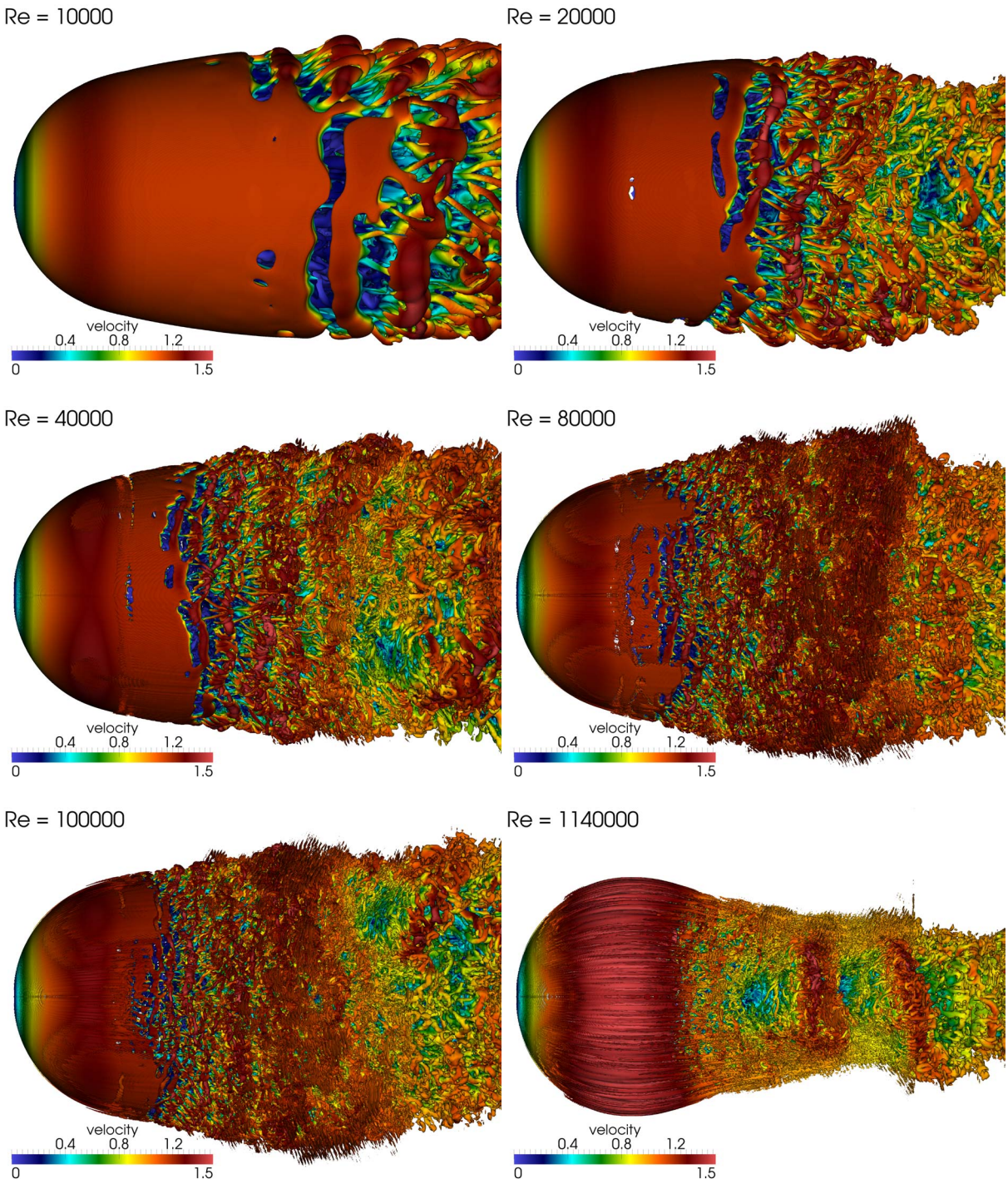

Figure 5: The Q-criterion for various Reynolds numbers. The contour represents the location where vorticity dominates shear, which is a way to visualize vortices. The color represents the velocity scaled with the inlet velocity ($u_0 = 1$). It is observed that the vortices become smaller for larger Reynolds number. Our simulation resolves the wake only close to the sphere. For high Reynolds numbers it is observed that the vortices are getting larger with the grid being coarser in some distance from the sphere. The cumulant method remains stable even if the flow is severely under-resolved.

conclusion for the drag on the sphere. The drag values in the intermediate state show a large fluctuation spanning almost the difference from the high drag to the low drag value. We have to note here that our time series is too short to draw definite conclusions but they appear to support the theory of intermittent transition. It must be emphasized that intermittent transition with a potential large time scale of the fluctuations make acquiring accurate measures for the critical Reynolds number very difficult if not impossible. A considerable deviation between different simulations and different experiments is therefore inevitable. In our simulations the flow travelled the diameter of the sphere only about 17 times. Intermittent events that happen on a time scale one order of magnitude longer than the vortex shedding frequency would appear at most once in our time series.

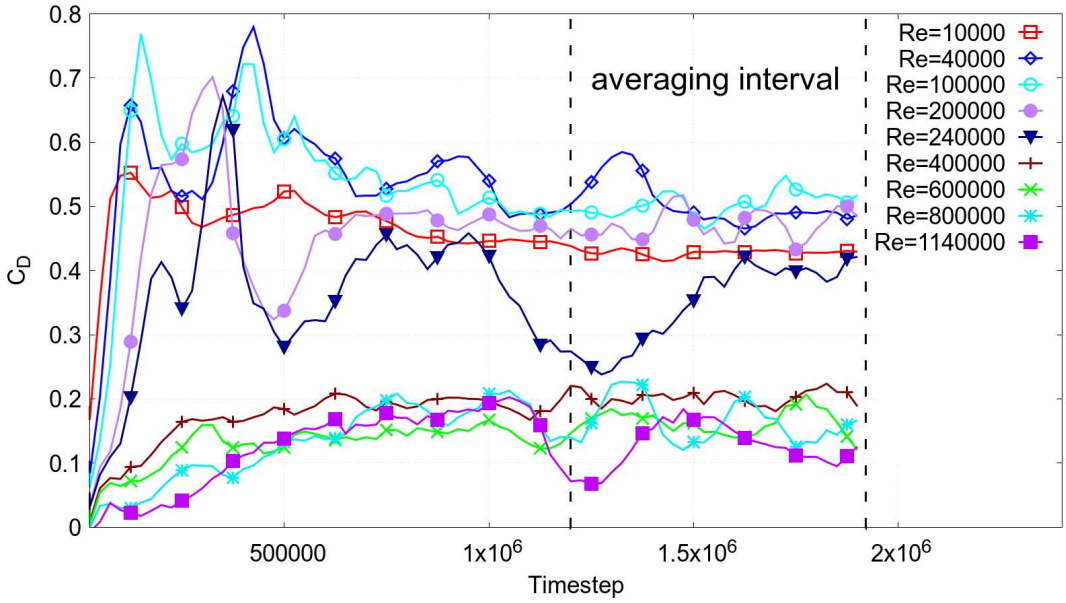

Figure 6: Time evolution of the measured c_D value for various Reynolds numbers using the medium resolution. It is seen that each averaged drag coefficient is subject to considerable uncertainty due to their large variation in time. The largest variations are seen for Reynolds number $Re = 240000$ where the drag coefficient is on the slope between the high and the low value. It is instructive to see that this intermediate c_D value does not appear to be stable in time. Instead the value swings between the upper and lower state, before and after the drag crisis. However, to confirm this behavior much longer time series should be recorded. The two vertical lines show the starting and ending time of the averaging procedure used to determine the average drag coefficient plotted in Fig. 2.

In Fig. 7 we compare the pressure distribution on the surface of the sphere to experimental results from Achenbach [12, 14].

5. Conclusions

In this paper we demonstrated the fidelity of the cumulant lattice Boltzmann method with fourth order accurate diffusion by applying it to the simulation of the drag crisis of a sphere. This test case was selected because it incorporates most of the difficulties of external aerodynamics of industrial relevance while still using a simple and generic shape for which sufficient data is available. The application of the optimized parameters was found to be necessary to capture the drag crisis on the given resolution. The non-optimized cumulant method shows encouraging results for sub-critical flows but it does not capture the drag crisis if the sphere is resolved by 512 lattice nodes. We note here that this does not put the validity of the non-optimized cumulant method into question. It just means that the computational efficiency of the non-optimized cumulant method is inferior to the optimized version as it requires higher resolution to obtain the same accuracy. It is to be expected that any correct numerical method would capture the drag crisis if the flow was sufficiently resolved. However, providing such high resolutions is extremely difficult. By increasing the convergence order for the diffusion, the optimized cumulant method offers a way to simulate highly turbulent flows

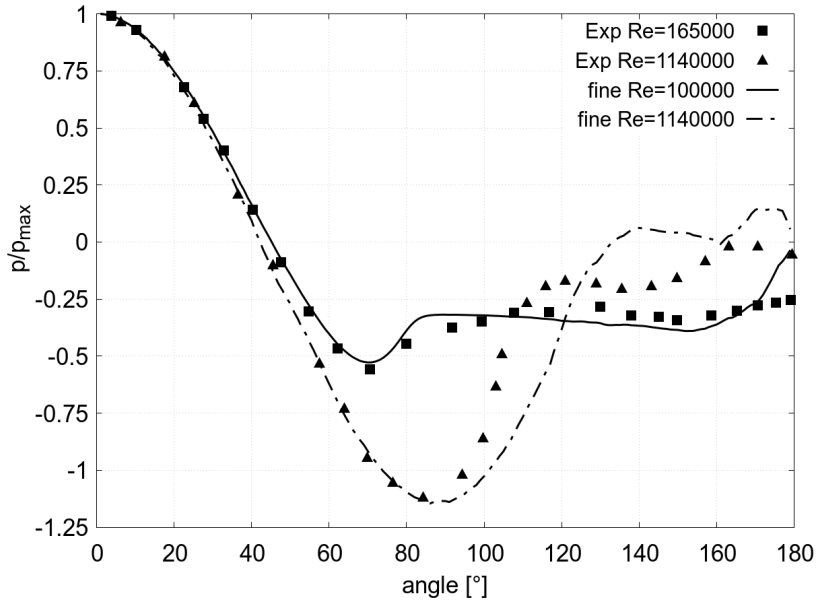

Figure 7: The distribution of pressure versus the polar angle. The simulation data was averaged in space but not in time and this is the cause of the strong residual fluctuations observed. The data of the experiment was obtained from Achenbach [12, 14]. The pressure distribution before the drag crisis is known to depend only very weakly on the Reynolds number. Similar curves where obtained for all sub-critical Reynolds numbers (no figure).

at a significantly reduced computational cost when compared with other lattice Boltzmann methods. For this to be possible, the method needs to be stable and accurate at the same time.

Even though we are not the first to present a parametrization of the lattice Boltzmann method for fourth order accuracy [7], our result is the first such parametrization that is highly relevant for the simulation of turbulent flow as it possesses the following attributes [1]:

- The method employs the standard D3Q27 stencil.
- It is general and isotropic in the sense that it does not depend on the direction of the flow or the type of the flow.
- It is derived under fully transient assumptions, i.e. it is not restricted to steady flow.
- The parametrization of the diffusion does not interfere with the accuracy order of the advection.
- The remaining influence that the parametrization has on advection is found to be positive [1], i.e. errors in advection are smaller for the optimized cumulant method than for the non-optimized method and they are significantly smaller than for the BGK method.
- The parametrization is valid for arbitrarily low viscosities.
- The parametrization does not require a change to the speed of sound of the original cumulant method which would deteriorate Galilean invariance.
- While the parametrization makes the cumulant method slightly less stable, it is possible to apply a limiter to the third order cumulants that stabilizes the method without interfering with the fourth order accuracy.
- The computational cost is identical (within 2%) to that of the non-optimized cumulant method.

Beside their obvious relevance for industrial applications in computational fluid dynamics, our results answer several academic questions.

In the past it appeared to be a matter of taste whether the availability of relaxation parameters for the ghost moments in same lattice Boltzmann models is an advantage or a disadvantage. In fact, the most prominent advantage of the single relaxation time or BGK lattice Boltzmann method is that the user does not need to decide on the rates of ghost moments. With a unique solution for the relaxation rates derived from the linearized leading error, as presented in this series of papers, the uncertainty in these rates has been removed. That is, the parameters are no longer free, they are known and they do not dependent on the flow under consideration. With this the fundamental question of how to chose the parameters has been mostly answered. Albeit we have to admit that our result covers only the relaxation rates of third order cumulants and the relaxation rates of fourth, fifth and sixth order cumulants are still undetermined. These rates can still be used for other types of optimization.

The case independent determination of the optimal relaxation rates based on accuracy should bring an end to the debate of whether the ghost modes should be chosen simply based on stability arguments. For example, the concept of so-called entropic lattice Boltzmann methods [41] is entirely built on the argument of stability and never addresses issues of accuracy. In fact, entropic lattice Boltzmann methods are frequently advertised for their property to converge to the BGK method [42, 43], or to provide the *same* accuracy as the BGK method at a significantly better stability. In contrast to this, the method presented here is not only stable for flows at very high Reynolds numbers, it also offers markedly better accuracy than the BGK method, even at a higher order of convergence, for the diffusion.

In a more general framework, compared to other weakly compressible methods applicable to the Navier-Stokes equation, the current result also provides an answer to the question why it is preferable to discretize an equation with four unknown variables with a much larger set of discrete velocities. In fact, if the so-called ghost modes were entirely irrelevant, the lattice Boltzmann method would have to be judged as being extremely inefficient, at least in terms of the required number of primitive variables. However, if these additional pieces of information can be employed to increase the convergence order of the method, as done here, their existence is completely justified. It is close to impossible that any numerical method will ever be found that obtains fourth order accuracy by accessing only the macroscopic variables at directly neighboring nodes once per time step. In order to obtain fourth order accuracy, finite difference methods have to employ much larger stencils than the one used for the lattice Boltzmann method.

Finally we have to note that the subject of fourth order accurate advection has not been discussed in this paper, even though we showed preliminary results in the first part of the series [1]. Combining fourth order accurate advection with fourth order accurate diffusion still poses some challenges which we will address in future research.

Acknowledgments

We thank Hussein Ali Hussein for proofreading the early manuscript and Jon McCullough for the final proofreading and many usefull suggestions. The research was funded by the TU Braunschweig. Most simulation results presented here were obtained on the compute cluster "Ludwig" of the Department of Architecture, Civil Engineering and Environmental Engineering of the TU Braunschweig until the last minutes before Ludwig was decommissioned.

Ludwig ∗ March 25th 2010 † March 8th 2017

Rest In Pieces.

References

[1] M. Geier, A. Pasquali, M. Schönherr, Parametrization of the cumulant lattice boltzmann method for fourth order accurate diffusion part i: derivation and validation, submitted to Journal of Computational Physics (2017).

[2] M. Geier, M. Schönherr, A. Pasquali, M. Krafczyk, The cumulant lattice boltzmann equation in three dimensions: Theory and validation, Computers & Mathematics with Applications 70 (4) (2015) 507 – 547. doi:http://dx.doi.org/10.1016/j.camwa.2015.05.001.
URL http://www.sciencedirect.com/science/article/pii/S0898122115002126

[3] E. K. Far, M. Geier, K. Kutscher, M. Krafczyk, Distributed cumulant lattice boltzmann simulation of the dispersion process of ceramic agglomerates, J. Comput. Meth. in Science and Engineering 16 (2016) 231–252.

[4] X. Yang, Y. Mehmani, W. A. Perkins, A. Pasquali, M. Schönherr, K. Kim, M. Perego, M. L. Parks, N. Trask, M. T. Balhoff, M. C. Richmond, M. Geier, M. Krafczyk, L.-S. Luo, A. M. Tartakovsky, T. D. Scheibe, Intercomparison of 3d pore-scale flow and solute transport simulation methods, Advances in Water Resources 95 (2016) 176 – 189, pore scale modeling and experiments. doi:http://dx.doi.org/10.1016/j.advwatres.2015.09.015.
URL http://www.sciencedirect.com/science/article/pii/S0309170815002225

[5] E. K. Far, M. Geier, K. Kutscher, M. Krafczyk, Simulation of micro aggregate breakage in turbulent flows by the cumulant lattice boltzmann method, Computers & Fluids 140 (2016) 222 – 231. doi:http://dx.doi.org/10.1016/j.compfluid.2016.10.001.
URL http://www.sciencedirect.com/science/article/pii/S0045793016302936

[6] A. Pasquali, M. Schönherr, M. Geier, M. Krafczyk, Simulation of external aerodynamics of the drivaer model with the lbm on gpgpus, Parallel Computing: On the Road to Exascale (2016) 391–400.
[7] F. Dubois, P. Lallemand, Towards higher order lattice boltzmann schemes, Journal of Statistical mechanics: theory and experiment 2009 (06) (2009) P06006.
[8] M. Geier, A. Pasquali, Fourth order galilean invariance for the lattice boltzmann method, submitted to Computers and Fluids (2017).
[9] G. Eiffel, Nouvelles recherches sur la rsistance de l'air et l'aviation faites au laboratoire d'Auteuil, Paris, H. Dunod et E. Piant, 1914.
[10] C. Wieselberger, Der luftwiderstand von kugeln, Zeitschrift f. Flugtechnik u. Motorluftschiffart (1914) 140.
[11] A. Roshko, Experiments on the flow past a circular cylinder at very high reynolds number, Journal of Fluid Mechanics 10 (3) (1961) 345356. doi:10.1017/S0022112061000950.
[12] E. Achenbach, Experiments on the flow past spheres at very high reynolds numbers, Journal of Fluid Mechanics 54 (3) (1972) 565575. doi:10.1017/S0022112072000874.
[13] O. Cadot, A. Desai, S. Mittal, S. Saxena, B. Chandra, Statistics and dynamics of the boundary layer reattachments during the drag crisis transitions of a circular cylinder, Physics of Fluids 27 (1). doi:http://dx.doi.org/10.1063/1.4904756.
URL http://scitation.aip.org/content/aip/journal/pof2/27/1/10.1063/1.4904756
[14] G. Constantinescu, K. Squires, Numerical investigations of flow over a sphere in the subcritical and supercritical regimes, Physics of Fluids 16 (5) (2004) 1449–1466. doi:http://dx.doi.org/10.1063/1.1688325.
URL http://scitation.aip.org/content/aip/journal/pof2/16/5/10.1063/1.1688325
[15] M. Muto, M. Tsubokura, N. Oshima, Negative magnus lift on a rotating sphere at around the critical reynolds number, Physics of Fluids (1994-present) 24 (1) (2012) 014102.
[16] O. Lehmkuhl, I. Rodrguez, R. Borrell, J. Chiva, A. Oliva, Unsteady forces on a circular cylinder at critical reynolds numbers, Physics of Fluids 26 (12). doi:http://dx.doi.org/10.1063/1.4904415.
URL http://scitation.aip.org/content/aip/journal/pof2/26/12/10.1063/1.4904415
[17] G. Chopra, S. Mittal, The intermittent nature of the laminar separation bubble on a cylinder in uniform flow, Computers & Fluids (2016) –doi:http://dx.doi.org/10.1016/j.compfluid.2016.06.017.
URL http://www.sciencedirect.com/science/article/pii/S004579301630202X
[18] M. Namburi, S. Krithivasan, S. Ansumali, Crystallographic lattice boltzmann method, Nature Scientific Reports 6 (2016) 27172.
[19] T. Kawamura, H. Takami, K. Kuwahara, Computation of high reynolds number flow around a circular cylinder with surface roughness, Fluid Dynamics Research 1 (2) (1986) 145 – 162. doi:http://dx.doi.org/10.1016/0169-5983(86)90014-6.
URL http://www.sciencedirect.com/science/article/pii/0169598386900146
[20] M. Schönherr, M. Geier, M. Krafczyk, Non-uniform lb simulations on gpus, in: ICMMES 2010, 2010.
[21] M. Geier, A. Greiner, J. G. Korvink, Cascaded digital lattice Boltzmann automata for high reynolds number flow, Phys. Rev. E 73 (2006) 066705. doi:10.1103/PhysRevE.73.066705.
[22] P. Asinari, Generalized local equilibrium in the cascaded lattice Boltzmann method, Phys. Rev. E 78 (2008) 016701. doi:10.1103/PhysRevE.78.016701.
URL http://link.aps.org/doi/10.1103/PhysRevE.78.016701
[23] M. Geier, De-aliasing and stabilization formalism of the cascaded lattice boltzmann automaton for under-resolved high reynolds number flow, INTERNATIONAL JOURNAL FOR NUMERICAL METHODS IN FLUIDS 56 (8) (2007) 1249–1254. doi:10.1002/fld.1634.
[24] M. Geier, A. Greiner, J. G. Korvink, Bubble functions for the lattice Boltzmann method and their application to grid refinement, The European Physical Journal Special Topics 171 (1) (2009) 173–179. doi:10.1140/epjst/e2009-01026-6.
[25] M. Schönherr, K. Kucher, M. Geier, M. Stiebler, S. Freudiger, M. Krafczyk, Multi-thread implementations of the lattice Boltzmann method on non-uniform grids for cpus and gpus, Comput. Math. Appl. 61 (12) (2011) 3730–3743. doi:10.1016/j.camwa.2011.04.012.
[26] K. Konstantin, M. Geier, M. Krafczyk, Multiscale simulation of turbulent flow interacting with porous media based on advanced massively parallel lbm models, submitted to Computers and Mathematics with Applications (2017).
[27] M. Geier, M. Schönherr, Esoteric twist: An efficient in-place streaming algorithmus for the lattice boltzmann method on massively parallel hardware, Computation 5 (2). doi:10.3390/computation5020019.
URL http://www.mdpi.com/2079-3197/5/2/19
[28] A. Pasquali, M. Geier, M. Krafczyk, LBMHexMesh: an OpenFOAM based grid generator for the Lattice Boltzmann Method (LBM), 7th Open Source CFD Int. Conf.
[29] A. Pasquali, Enabling the cumulant lattice Boltzmann method for complex CFD engineering problems, Ph.d. thesis, Technische Universität Braunschweig (2016).
[30] H. Schlichting, Boundary layer theory, part 1: Laminar flows, Tech. rep., Luftfahrtforschungsanstalt Hermann Goering; Brunswick, Germany (1949).
[31] N. Tetervin, Theoretical distribution of laminar-boundary-layer thickness, boundary-layer Reynolds number and stability limit, and roughness Reynolds number for a sphere and disk in incompressible flow, National Advisory Committee for Aeronautics, 1958.
[32] J. Hoffman, Simulating drag crisis for a sphere using skin friction boundary conditions, in: ECOMAS CFD 2006: Proceedings of the European Conference on Fluid Dynamics, TU Delft, The Netherlands, 2006.
[33] J. Hoffman, Simulation of turbulent flow past bluff bodies on coarse meshes using general galerkin methods: Drag crisis and turbulent euler solutions, Computational Mechanics 38 (4) (2006) 390–402. doi:10.1007/s00466-006-0053-x.
URL http://dx.doi.org/10.1007/s00466-006-0053-x
[34] L. Prandtl (Ed.), Strmungsmechanik Bd. 5, Universittsverlag Gttingen, 2009.
[35] V. Bakic, Experimental investigation of turbulent flows around a sphere, Ph.D. thesis, Technische Universitt Hamburg-Harburg (2002).
[36] F. A. Morrison, An Introduction to Fluid Mechanics, Cambridge University Press, 2013.
[37] J. Almedeij, Drag coefficient of flow around a sphere: Matching asymptotically the wide trend, Powder Technology 186 (3) (2008) 218 – 223. doi:http://dx.doi.org/10.1016/j.powtec.2007.12.006.
[38] R. Mei, D. Yu, W. Shyy, L.-S. Luo, Force evaluation in the lattice Boltzmann method involving curved geometry, Phys. Rev. E 65 (2002)

041203.
[39] J. Hunt, A. Wray, P. Moin, Eddies, streams, and convergence zones in turbulent flow, in: Center for Turbulence Research Proceedings of the Summer Program 1988, 1988.
[40] J. J. Miau, H. W. Tsai, Y. J. Lin, J. K. Tu, C. H. Fang, M. C. Chen, Experiment on smooth, circular cylinders in cross-flow in the critical reynolds number regime, Experiments in Fluids 51 (4) (2011) 949–967. doi:10.1007/s00348-011-1122-2.
URL http://dx.doi.org/10.1007/s00348-011-1122-2
[41] B. M. Boghosian, J. Yepez, P. V. Coveney, A. Wager, Entropic lattice boltzmann methods, in: Proceedings of the Royal Society of London A: Mathematical, Physical and Engineering Sciences, Vol. 457, The Royal Society, 2001, pp. 717–766.
[42] O. Malaspinas, M. Deville, B. Chopard, Towards a physical interpretation of the entropic lattice boltzmann method, Physical Review E 78 (6) (2008) 066705.
[43] F. Tosi, S. Succi, An introduction to entropic lattice boltzmann scheme, SIMAI e-Lecture Notes 1.